Stationary human Presence Detection using 24 GHz radar

Yunki Yau, *SID 200491720*

***Abstract*— Stationary human presence detection without the use of optical or infrared imaging is essential in scenarios where privacy, visibility, or environmental constraints preclude line-of-sight access to the target. This study presents a custom software interface developed for stationary human presence detection using a commercial 24 GHz frequency-modulated continuous-wave (FMCW) radar module. The bespoke Python program enables real-time visualisation of analog-to-digital converter (ADC) signals, fast Fourier transform (FFT) spectra, and phase tracking within a 1.3–1.7 m detection range, with on-demand data recording for subsequent analysis. Using this platform, two complementary detection strategies were implemented and compared: a conventional threshold-based classifier operating on spectral features derived from the phase-variation spectrum, and an unsupervised machine-learning (ML) classifier combining principal component analysis (PCA) with an Isolation Forest model.**

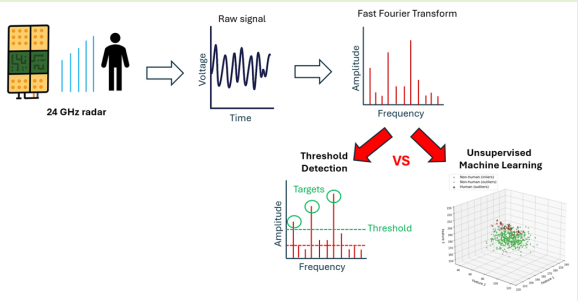

In a 60 sample (44 development, 16 evaluation) dataset comprising of human and non-human targets in both indoor and outdoor environments, including static and oscillating reflectors, the conventional threshold-based classifier achieved higher accuracy (68.8 %) in stationary human presence detection compared to the unsupervised ML model (56.2 %). The results of this study highlight the continued relevance of classical threshold-based signal-processing methods alongside modern machine-learning approaches, even in dynamic outdoor conditions, and establishes a flexible, open-source framework for further experimentation in low-power radar-based vital-sign and presence detection systems.

***Index Terms*— Frequency Modulated Continuous Wave (FMCW) radar, threshold detection, Principal Components Analysis (PCA), Isolation Forest, machine learning.**

I. Introduction

DETECTING the presence of people who are stationary - those who are motionless or still - has many practical applications, from monitoring residents in aged care, to locating unconscious victims during search and rescue, and identifying concealed persons in law enforcement or defence operations [1], [2]. In these contexts, optical or infrared imaging is either inappropriate or ineffective due to physical obstructions that prevent line-of-sight access and reliance on environmental illumination or thermal penetration [3].

Frequency Modulated Continuous Wave (FMCW) radar, by contrast, can operate through (non-metallic) barriers and functions independently of ambient lighting conditions [3]. Even when a person remains still, subtle physiological motions occur, such as respiratory chest displacement or even the rhythmic contractions of the heart [4]. Radars operating at 24 GHz are particularly suited for detecting these micro-motions or 'micro-Doppler' signatures, with wavelengths that are able to resolve millimetre-scale displacement while remaining non-ionising for human exposure [5]. A growing body of literature suggests that 24 GHz radar achieves high accuracy in detecting stationary human presence, albeit in controlled, indoor laboratory settings [6]–[8].

Conventional radar signal processing typically relies on threshold-based classification of spectral or temporal features extracted from the returned radar signal, and approaches such as constant-false-alarm-rate (CFAR) detection and root-mean-square (RMS) amplitude thresholding are commonly used to distinguish target presence from noise [3], [9]. These methods are computationally efficient and physically interpretable, but fundamentally rely on differences in wave reflection between the target and environment, and can thus be difficult to interpret in cluttered or dynamic environments.

More recently, machine learning (ML) has emerged as a complementary approach for radar-signal processing, offering data-driven adaptability that may make it more robust to complex environments [10], [11]. Unsupervised ML models - algorithms that do not require labelled training data - are particularly adaptable to environmental variability, as it independently infers patterns in a dataset that may be obscure to human interpretation [12]. The potential of ML-based radar signal processing to enhance stationary human presence detection in particular, remains an active and evolving area of research [13].

Submitted: 31st October 2025
Yunki Yau, SID 200491720, SCDL3992, Semester 2, 2025. yyau2516@uni.sydney.edu.au

TABLE I

RADAR OPERATING PARAMETERS

Parameter (symbol)	Value
Operating frequency range (f_1–f_2)	23.10 - 26.18 GHz
Modulation bandwidth ($B = f_2 - f_1$)	3.078 GHz
Ramp time (t_{ramp})	0.84 ms
Chirp slope ($S = B/t_{\mathrm{ramp}}$)	3.66 THz/s
ADC sampling rate (f_s)	0.675 MS/s
Samples per chirp (N)	512
FFT size (N_{FFT})	512
Windowing	Blackman-Harris
Output mode	continuous complex (I/Q) output
Gain control (AGC)	Enabled
Host interface	UART @ 230,400 baud

A. Aims

In this study, we aimed to evaluate the effectiveness of classical threshold-based signal processing and unsupervised machine learning approaches for stationary human presence detection using a 24 GHz radar system. The work was designed as a proof-of-concept comparison conducted under both indoor and outdoor conditions to assess the practicality and adaptability of each method.

The specific objectives were to:

1. Configure an off-the-shelf commercial 24 GHz radar module for stationary human presence detection.

2. Develop and implement two detection pipelines: a conventional threshold-based classifier and an unsupervised machine learning classifier for identifying stationary human targets positioned at distances representative of typical short-range indoor sensing (approximately 1.3 – 1.7 m).

3. Compare the performance of both approaches in terms of detection accuracy, sensitivity and specificity.

II. METHODS

A. Radar Configuration

A commercial 24 GHz Frequency-Modulated Continuous-Wave (FMCW) radar evaluation kit (SiRad Easy r4 baseboard with TRX_024_046 front-end, Indie Semiconductor FFO GmbH, Germany) was employed as the sensing platform. The system consists of a baseband processing board supporting interchangeable radar front-ends and an integrated microcontroller for frequency ramp generation, signal conditioning, and analog-to-digital conversion (ADC) [14]. The front-end incorporates a single-channel IQ transceiver operating nominally between 23.1 GHz and 26.2 GHz, with separate transmit (TX) and receive (RX) patch antennas mounted on a 98 × 40 mm PCB [15]. The module was controlled via a USB serial connection to a host computer running a custom Python control and data-logging interface (Section II-C).

1) Operating Mode and Frequency Ramp Parameters: The radar was operated in continuous FMCW (CPL) mode, configured through serial commands transmitted using the SiRad protocol (see Protocol Description Easy r4, Indie Semiconductor) [16]. The key operating parameters are summarised in Table I.

The on-board phase-locked-loop (PLL) synthesiser generated the frequency modulation ramps, and the radar's internal amplifier–filter network conditioned the in-phase (I) and quadrature (Q) baseband signals before digitisation [16]. Automatic-gain control (AGC) was left enabled at the default setting to maintain optimal receiver dynamic range during data acquisition.

TABLE II

MEASUREMENT RECORDINGS COLLECTED FOR THRESHOLD DETECTION AND MACHINE LEARNING CLASSIFIERS

Dataset	Negative (Non-human)	Positive (human Present)
Development	30	14
Evaluation	8	8

2) Signal Interface and Data Acquisition: Communication between the radar and host PC was achieved through a UART-to-USB serial interface operating at 230 400 baud I [17]. Raw I/Q samples were streamed to the host computer and captured using a custom Python program (`ADC_FFTs_07OCT.py`) developed for this work, which transmitted the serial configuration commands corresponding to the operating parameters listed in Table I. The source code is publicly available in the project repository [18].

The received I and Q data were stored in binary arrays for subsequent conversion and processing (Section II-C).

B. Data Acquisition

Radar measurements were recorded over three separate days across three distinct environments: a small office, a larger indoor area, and an outdoor space 1. *Positive* measurements were defined as those containing a human target positioned within 1.3–1.7 m of the radar, either seated or standing, and at rest or immediately following calisthenic exercise to elevate heart and respiratory rates. *Negative* measurements were defined as those without a human target within 1.3–1.7 m, but which could include static or oscillating non-human reflectors at distances of 1.5, 2.0, 2.5, or 3.0 m, or human targets positioned at 2.0, 2.5, or 3.0 m. A nominal range of 1.5 m was chosen for positive cases so that a standing average adult would fill the radar cross-section of the TRX_024_046 front-end (approximately 1 x 2 m), which was calculated using the standard aperture-size Half-Power Beamwidth (HPBW) approximation for rectangular apertures [3]:

$$\mathrm{HPBW} \approx 0.885\,\frac{\lambda}{D}\ \text{radians} \tag{1}$$

λ denotes the operating wavelength of the radar, and D is the effective linear dimension of the transmitting aperture.

Three individuals were used as human targets across the recording sessions. An oscillating non-human target was constructed by attaching a tin container lid to the top of a Dyson AMO6 desk fan (Dyson, UK), which oscillated laterally at approximately 0.1 Hz (Fig. 1b). The duration of each measurement was approximately 3 minutes to capture multiple cycles of physiological micro-motions. In total, 60 measurements were recorded, comprising 44 recordings (both positive and negative) used for classifier development, and 16 recordings reserved for the evaluation dataset (Table II).

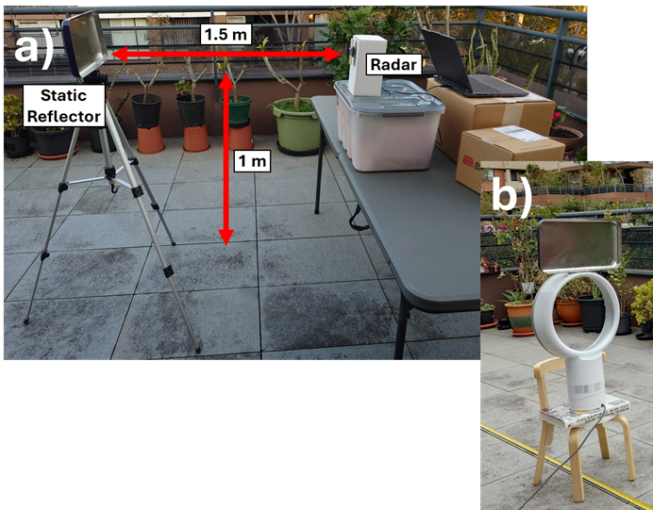

Fig. 1. Representative data acquisition setup. a) An outdoor measurement setup with the SiRad Easy r4 radar module on the right positioned 1 m from the ground with a static reflector (a tin container lid) mounted on a tripod 1.5 m away. b) The oscillating non-human reflector. This configuration was used to generate controlled periodic micro-motion signatures for validation of detection algorithms.

C. Python-Based Signal Processing and Feature Extraction

A bespoke Python program was developed to control data acquisition and perform real-time signal processing using the `serial`, `numpy`, and `matplotlib` libraries. Upon initialisation, the program transmitted the configuration commands `!S150B2812`, `!F000168F0`, `!P00000603`, and `!B2452C122` to the radar via a UART interface.

Continuous streaming of the in-phase (I) and quadrature (Q) analog-to-digital converter (ADC) outputs was performed at a sampling rate of $f_s = 675$ kS/s Table I. The Python interface displayed four concurrent plots in real time: the time-domain I and Q channels, the individual FFT spectra of I and Q, the complex spectrum $|\mathrm{FFT}(I + jQ)|$, and the unwrapped temporal phase $\phi(t)$ extracted from a defined range gate Fig. 2. The range–bin conversion ΔR_{bin} was determined from the chirp slope S using:

$$\Delta R_{\mathrm{bin}} = \frac{c\, f_s}{2S\, N_{\mathrm{FFT}}}, \tag{2}$$

where c is the speed of light and $N_{\mathrm{FFT}} = 512$ was the FFT length. Range gating between 1.3–1.7 m was implemented by masking FFT bins corresponding to this interval.

Each FFT frame was windowed using a 4-term Blackman–Harris function prior to spectral analysis. A weighted complex sum $Z(t)$ within the range gate was computed:

$$Z(t) = \sum_{k=k_l}^{k_h} w_k(t) X_k(t), \tag{3}$$

where X_k is the complex FFT coefficient of the kth bin (between the low (k_l) and high (k_h) frequency bins of the 1.3–1.7 m range of interest)) and w_k is the magnitude-based weighting factor given by:

$$w_k(t) = \frac{|X_k(t)|}{\sum_{i=k_l}^{k_h} |X_i(t)|}, \tag{4}$$

The unwrapped instantaneous phase $\phi(t) = \arg(Z)$ was displayed in real time and logged for subsequent analysis.

Each recording was saved as a comma-separated values (CSV) file containing time (t), wrapped and unwrapped phase, the weighted complex magnitude $|Z|$, and 257 positive-frequency FFT bins with their corresponding range annotations. The program enabled concurrent data visualisation, phase tracking, and on-key recording using lightweight keyboard bindings (`R` to record, `Q` to quit).

The full Python implementation for radar control, data acquisition, and feature extraction (`ADC_FFTS_07OCT.py`) is available in the project repository [18].

D. Detection Algorithms

Two detection pipelines were developed to evaluate stationary human presence under indoor and outdoor conditions: a conventional threshold-based detector and an unsupervised machine-learning classifier. Both approaches operated on the same CSV feature set as previously mentioned.

1) Threshold-Based Detection: The threshold-based detector operated on spectral features computed from the unwrapped phase time series ($\phi_(t)$) extracted within the 1.3–1.7 m range gate (Section II-C). The unwrapped phase sequence was uniformly resampled at a slow-time rate of $f_s = 10$ Hz and segmented using Welch's method to obtain a smoothed power spectral density (PSD) $S_\phi[k]$ (Fig. 3). Specifically, the Welch PSD was computed using a 256-sample Blackman–Harris window ($L = 256$), corresponding to a 25.6 s window length, with 50% overlap between segments. The resulting discrete frequency grid was

$$\begin{aligned} f_k &= k\,\Delta f, \\ \Delta f &= \frac{f_s}{L} = 0.039 \text{ Hz}, \\ k &\in \{0, 1, \ldots, L/2\}. \end{aligned}$$

From $S_\phi[k]$, four candidate features were evaluated as univariate decision variables within the 0.05–1.00 Hz analysis band: spectral flatness (SF), spectral crest (SC), centroid frequency (f_c), and phase variance (σ_ϕ^2) [19], [20]. This frequency range was selected to capture low-frequency spectral energy associated with quasi-periodic physiological micro-motions such as respiration, while excluding slow drifts and higher-frequency noise components. The four candidate features were defined as:

a) Spectral flatness (SF).: Defined as the ratio of geometric to arithmetic mean of the PSD:

$$\mathrm{SF} = \frac{\exp\left(\frac{1}{M}\sum_{k=0}^{M-1} \ln\big(S_\phi[k] + \varepsilon\big)\right)}{\frac{1}{M}\sum_{k=0}^{M-1} S_\phi[k]}, \tag{5}$$

where M is the number of PSD bins in the analysis band and ε is a small constant (e.g., 10^{-12}) to avoid $\ln 0$.

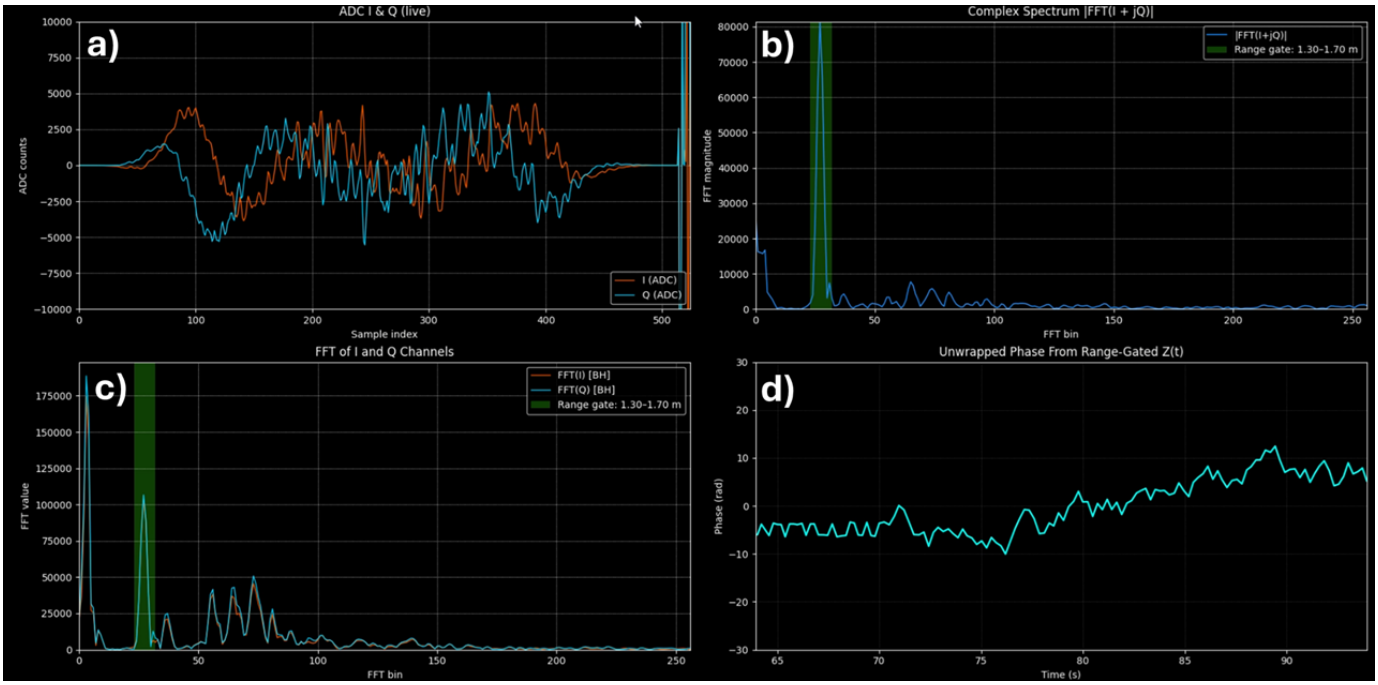

Fig. 2. Interface of custom Python program developed for real-time radar signal acquisition and processing. (a) Time-domain display of in-phase (I) and quadrature (Q) ADC channels. (b) Fast Fourier transform (FFT) magnitude spectra of the individual I and Q signals. (c) Complex magnitude spectrum $|\mathrm{FFT}(I + jQ)|$ (d) Unwrapped temporal phase $\phi_(t)$ extracted from the weighted complex sum within the range gate of 1.3–1.7 m (the green highlighted bar in (b) and (c)). The interface enabled simultaneous data visualisation, phase tracking, and on-key recording in real time.

b) Spectral crest (SC).: Defined as the peak-to-mean ratio of the PSD:

$$\mathrm{SC} = \frac{\max\limits_{0\le k<M-1} S_\phi[k]}{\dfrac{1}{M}\displaystyle\sum_{k=0}^{M-1} S_\phi[k]}. \tag{6}$$

c) Centroid frequency (f_c).: The power-weighted mean frequency (spectral centroid):

$$f_c = \frac{\displaystyle\sum_{k=0}^{M-1} f_k\, S_\phi[k]}{\displaystyle\sum_{k=0}^{M-1} S_\phi[k]}. \tag{7}$$

d) Phase variance (σ_ϕ^2).: By Parseval's relation, the variance of $\phi(t)$ over the analysis band equals the area under the PSD, where Δf denotes the discrete frequency bin width [20]:

$$\sigma_\phi^2 = \sum_{k=0}^{M-1} S_\phi[k]\,\Delta f. \tag{8}$$

For each feature $x \in \{\mathrm{SF}, \mathrm{SC}, f_c, \sigma_\phi^2\}$, a scalar threshold T_x was selected by iterating over candidate values on the development dataset to maximise *Youden's J* index. Youden's J provides a single summary metric of the overall diagnostic effectiveness of a binary classifier, defined as the sum of sensitivity and specificity minus one [21]. A value of $J = 1$ represents perfect discrimination, whereas $J = 0$ corresponds to random chance [21].

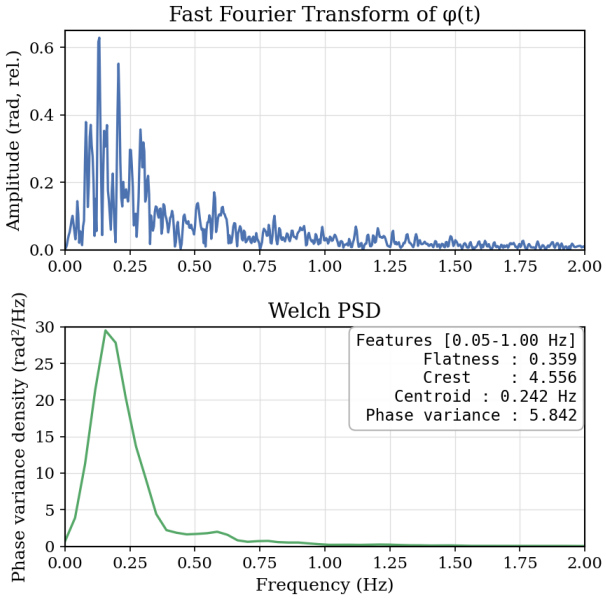

Fig. 3. A representative FFT and Welch PSD of $\phi(t)$ of a positive (human presence) radar recording. The Welch PSD effectively smooths the spectrum, facilitating the calculation of the four spectral features.

$$J(T_x) = \mathrm{Sensitivity}(T_x) + \mathrm{Specificity}(T_x) - 1 = \mathrm{TPR}(T_x) - \mathrm{FPR}(T_x), \tag{9}$$

where $\mathrm{TPR} = \frac{\mathrm{TP}}{\mathrm{TP+FN}}$ is the true–positive rate and $\mathrm{FPR} =$

$\frac{FP}{FP+TN}$ is the false–positive rate. The threshold search was automated in Python (`development_thresholds.py`); the implementation is available in the project repository [18].

2) Unsupervised Machine-Learning Classifier: An unsupervised anomaly-detection pipeline was developed using a combination of principal component analysis (PCA) and an isolation forest algorithm, implemented in `scikit-learn` (train_iforest.py, available at https://github.com/yunkiyau/stationary_presence_detection). The feature matrix comprised the 257 positive-frequency magnitude bins of the FFT computed from the complex signal $I + jQ$, representing the combined spectral information of both quadrature channels. Each sample corresponded to approximately three minutes of phase data, yielding around 550 discrete time points per recording.

The PCA was first applied to reduce feature dimensionality and decorrelate the input space while retaining 95% of the total variance [22]. The transformed data were then used to train an isolation forest model, which learns the distribution of the majority ("Non-human") class without requiring labelled examples of the minority ("human present") class. The classifier was trained exclusively on negative samples from the development dataset, with an expected contamination rate of 10 %, representing the anticipated proportion of outliers [23]. The model assigns each sample an anomaly score s, inversely proportional to the average path length in the isolation trees [23]. After training, a detection was declared when s exceeded the decision boundary T_s determined from the 95th percentile of scores in the development set. This approach allowed the classifier to autonomously infer deviations from the baseline environment, with the purpose of capturing spectral and temporal perturbations associated with stationary human presence that are not easily discernible through manual analysis.

All models were evaluated using the independent evaluation dataset described in Table II, with performance metrics reported in terms of accuracy, sensitivity, and specificity (Section III-C).

III. Results

A. Threshold Feature Performance

Stationary human presence classification thresholds for four candidate spectral features—flatness, crest factor, spectral centroid, and phase variance—were iteratively optimized on the development dataset to maximize Youden's index, as described in Section II-D.1. The resulting feature distributions and corresponding optimal thresholds are shown in Fig. 4.

As illustrated, there was substantial overlap between the "human present" (orange) and "non-human" (blue) samples across most features, with only **phase variance** (Fig. 4b) exhibiting discriminability appreciably above chance. The optimized threshold for phase variance corresponded to a cutoff value of **phase variance** ≥ 9.31 a.u., yielding a sensitivity of 86 %, specificity of 87 %, and a maximum Youden's $J = 0.72$. This indicates that increases in low-frequency phase power, represented by the integrated area under the Welch power spectral density (PSD), were the most consistent spectral signature associated with human presence.

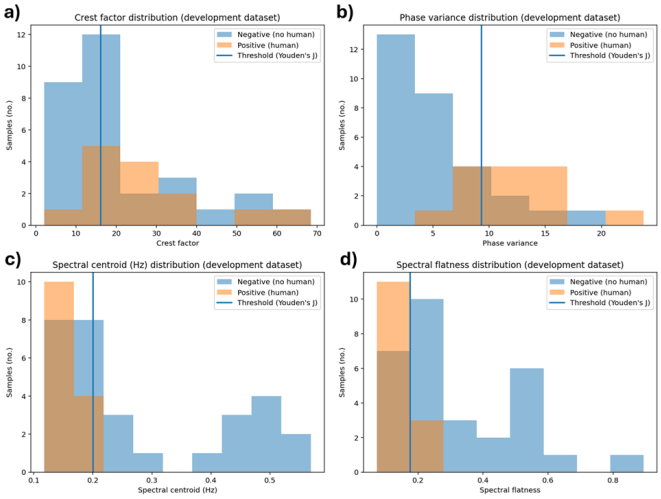

Fig. 4. Spectral feature threshold optimization using Youden's J statistic. (a) Crest factor: optimal threshold ≥ 16.15, $J = 0.39$; (b) Phase variance: ≥ 9.31, $J = 0.72$; (c) Spectral centroid: ≤ 0.20, $J = 0.53$; (d) Spectral flatness: ≤ 0.18, $J = 0.55$.

In contrast, the **spectral flatness** (Fig. 4d) and **spectral centroid** (Fig. 4c) features, with optimal thresholds of ≤ 0.18 a.u. and ≤ 0.20 a.u., respectively, achieved J values below 0.6, indicating poor separability between classes. The **crest factor** (Fig. 4a) performed worst overall, with $J < 0.4$.

These results indicate that among the tested spectral features, only **phase variance** carried discriminative information about the presence of stationary humans. Consequently, this feature alone was selected as the basis for the subsequent threshold-based classifier evaluated on the independent evaluation dataset (Section III-C).

B. Development of Unsupervised Machine-Learning Classifier

To verify the internal consistency of the trained model, the Isolation Forest was reapplied to the same 30 negative (*non-human*) development recordings used during training. The model classified 27 recordings as inliers and three as outliers, consistent with the 10 % contamination level specified during training. This result indicates that the model behaved as expected, defining a compact and stable baseline representation of normal radar spectra without exhibiting over-sensitivity to benign spectral variability.

Figure 5 shows the two-dimensional principal-component projection of the development dataset, coloured by the Isolation Forest anomaly score. The majority of samples formed a grouping of low-score points along the lower range of PC1, representing nominal background conditions. The three high-score outliers correspond to the false-positive detections, appearing as isolated points toward higher PCA 1 values. Their separation suggests that these recordings contained atypical spectral characteristics relative to the rest of the negative set.

Given the model's stable behaviour on the development data and limited FPR, it was adopted as the final unsupervised classifier for subsequent assessment on the independent evaluation dataset described in (Section III-C).

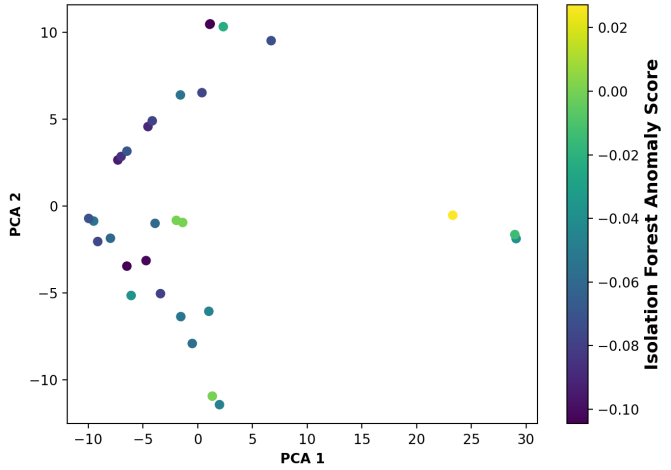

Fig. 5. Two-dimensional PCA projection of FFT-bin feature vectors from the development dataset, coloured by Isolation Forest anomaly score. High-score outliers correspond to the three false-positive detections within the negative training set. The Isolation Forest anomaly score is normalised so that the decision threshold lies at a score of zero.

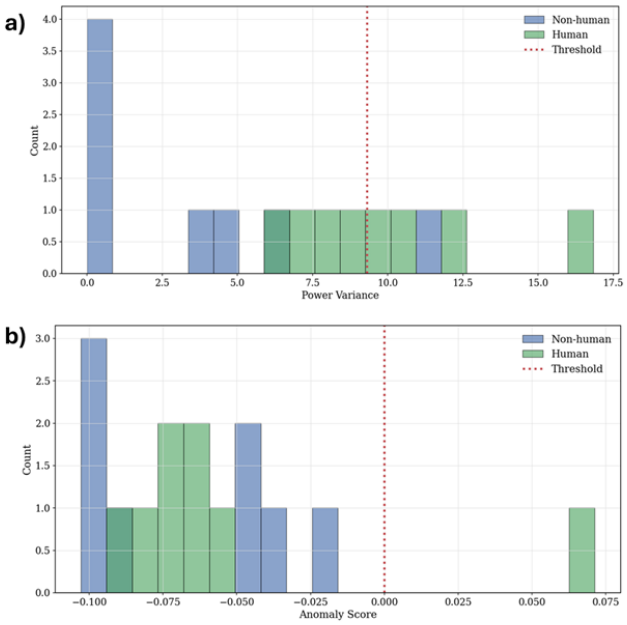

Fig. 6. Comparison of classifier performance on the evaluation dataset. (a) Power variance distribution for the threshold-based classifier. (b) Isolation Forest anomaly score distribution for the unsupervised machine-learning classifier. The red dashed line indicates the decision threshold separating *human present* and *Non-human* classifications.

C. Accuracy of Threshold Detection Versus Unsupervised ML for Stationary human Presence Detection

To assess comparative performance, both the threshold-based and unsupervised machine-learning classifiers were applied to the independent evaluation dataset containing 8 positive (*human present*) and 8 negative (*Non-human*) recordings. The resulting detection score distributions for each classifier are presented in Fig. 6. The upper histogram (a) shows the distribution of power variance values for the threshold classifier, while the lower histogram (b) shows the corresponding Isolation Forest anomaly scores. In both cases, the red dashed line indicates the respective decision threshold. The threshold classifier exhibited a broad spread of power variance values, with the majority of *human present* samples clustered around both sides of the decision boundary. *Non-human* samples largely had low power variance values. In contrast, the unsupervised model produced a large concentration of all samples below the detection threshold.

The classification outcomes for each model are summarised in the confusion matrices shown in Tables III and IV. The threshold-based detector achieved an accuracy of 68.8 %, with 50.0 % sensitivity and 87.5 % specificity, whereas the unsupervised Isolation Forest attained 56.2 % accuracy, 12.5 % sensitivity, and 100 % specificity. Although both classifiers produced similar confusion patterns, the threshold-based model achieved higher overall accuracy and sensitivity on this evaluation dataset. In contrast, the unsupervised Isolation Forest exhibited perfect specificity but lower sensitivity, reflecting its more conservative detection behaviour in this limited sample set.

TABLE III
THRESHOLD DETECTION CLASSIFIER CONFUSION MATRIX

	Predicted Negative	**Predicted Positive**
True Negative	30	14
True Positive	8	8

TABLE IV
MACHINE LEARNING CLASSIFIER CONFUSION MATRIX

	Predicted Negative	**Predicted Positive**
True Negative	30	14
True Positive	8	8

IV. DISCUSSION

In this exploratory proof-of-concept study, two approaches for stationary human presence detection were evaluated using a 24 GHz FMCW radar: a conventional threshold-based classifier and an unsupervised machine-learning model implemented as a principal component analysis (PCA) and Isolation Forest pipeline.

Substantial development work was undertaken to adapt the commercial off-the-shelf radar platform for the bespoke task of stationary human presence detection. The SiRad Easy r4 system was configured in continuous FMCW mode with a 3.08 GHz sweep bandwidth and a chirp slope of 3.66 THz/s, providing sub-centimetre range resolution suitable for short-range micro-motion sensing I. After configuration, a custom Python interface was then developed to control the radar via UART, perform real-time FFT processing of the complex baseband $(I + jQ)$ signal, and extract the unwrapped phase from a defined range gate between 1.3 m and 1.7 m. This range was chosen to simplify detection by ensuring that a stationary human target fully occupied the radar cross-section within the field of view.

The Python software enables real-time visualisation of I and Q channels, FFT spectra, and unwrapped phase, and supports on-demand recording, data logging, and phase tracking within the detection gate for subsequent analysis of target dynamics. The capture program and analysis scripts, including the development code for both classifiers presented in this work, are open-source and publicly available in the project repository [18].

Among the four candidate spectral features evaluated for the threshold-based classifier, only phase variance exhibited appreciable discriminative power on the development dataset Fig. 4. This outcome is likely because phase variance provides a broad measure of the total power in the low-frequency portion of the phase spectrum, thereby capturing temporal fluctuations associated with targets that are not completely static. Given that the spectral features were computed within the 0.05–1 Hz band, phase variance is directly attributable to micro-motions with frequencies typical of respiratory or postural movements. Consequently, it was selected as the sole feature for the prototype threshold-based detector.

In contrast, the machine-learning model (PCA–Isolation Forest) does not rely on a single physically interpretable feature of an individual radar return, but instead learns the statistical structure of the multidimensional FFT-derived feature space, identifying anomalous patterns within the overall distribution of radar spectra across the dataset. The model was trained exclusively on negative (*non-human*) recordings to learn a baseline representation of typical spectral characteristics, against which new radar data were subsequently evaluated. A positive detection is declared when a new feature-space pattern deviates significantly from this learned baseline. When reapplied to the development dataset, the model demonstrated stable and internally consistent behaviour, confirming that it had learned a coherent representation of background spectral variability suitable for subsequent evaluation on unseen data.

When applied to the independent evaluation dataset, both classifiers achieved modest performance, with the threshold-based approach exhibiting higher overall accuracy (68.8 % vs. 56.2 %) primarily due to its greater sensitivity (50.0 % vs. 12.5 %). As illustrated in Fig. 6a, a threshold of approximately > 5 a.u. would have correctly identified all *human-present* samples while misclassifying only two of eight *non-human* samples. This suggests that iterative manual tuning of a simple threshold-based detector is feasible even in small datasets that encompass diverse recording scenarios, including both indoor and outdoor environments with human, static and oscillating reflectors.

Both classifiers demonstrated high specificity (87.5 % for the threshold-based method and 100 % for the machine-learning model) but low sensitivity overall, indicating difficulty in identifying true stationary human presence. Several factors observed during data collection may explain this behaviour. In outdoor recordings, high wind conditions caused stationary reflectors to oscillate in place, producing apparent micro-motions similar to those of a stationary human. Additionally, wind-induced vibration of the radar module itself - despite its weighted base - introduced real-time fluctuations observable in $\phi(t)$ even during free-space measurements. The movement of clothing due to wind on human targets would also generate spurious low-frequency phase variations, potentially masking genuine physiological micro-motions. These effects likely caused the radar returns of true stationary humans to resemble those of static or oscillating non-human reflectors within the 1.3–1.7 m detection range, which were used as negative samples in both development and evaluation datasets. This would have effected both classifiers equally. The threshold-based detector encountered overlapping phase-variance distributions, and an overall reduced separability in FFT-derived feature spaces would have been observed by the PCA-Isolation Forest model.

Given the limited size of the development and evaluation datasets, a more constrained experimental design (e.g., indoor-only measurements) would likely have improved the discriminative performance of both approaches. For the PCA–Isolation Forest model, the use of a strict binary classification framework (*human present* vs. *no human within 1.3–1.7 m*) may have limited its capacity to exploit the nuanced structure of the data. Extending the model to multiple classes (e.g., *static reflector*, *oscillating reflector*, *human*, and *free space*) could allow the unsupervised algorithm to capitalise on its strength in recognising subtle, high-dimensional patterns that are not easily identifiable through manual analysis.

These findings build upon previous microwave-wavelength radar studies that have demonstrated reliable human detection under controlled indoor conditions [6]–[8]. In contrast to these prior works, the present study examined stationary human presence detection across both indoor and outdoor environments, experimentally showing that detection performance based on temporal phase variations deteriorates in dynamic settings, where micro-Doppler signatures are not uniquely human in origin. Under such conditions, machine-learning approaches remain a promising avenue, as they can exploit multiple spectral and statistical characteristics of the radar signal rather than relying on a single, hand-crafted feature.

A. Practical Implications

For short-range stationary human presence detection tasks where interpretability and computational efficiency are prioritised, a single-feature threshold based on phase variance offers a simple yet effective approach that can be iteratively optimised. Such methods are particularly well-suited to semi-controlled indoor environments, where radar-based presence monitoring has already seen successful deployment in healthcare settings [24], [25]. The present findings also indicate that deployment in more dynamic environments remain feasible, provided that careful consideration be given to iterative threshold tuning and periodic system calibration to account for varying baseline environmental conditions.

Each recording in this study was three minutes in duration, which enabled robust estimation of phase variance; however, practical implementations requiring rapid or real-time detection would necessitate inference over shorter time windows and additional validation would be required in this aspect. Furthermore, practical deployment of a radar-based stationary human presence detector would necessitate rigorous specifi-

cation of environmental operating parameters, including temperature, wind conditions, and vibration tolerance, to maintain performance consistency across diverse field environments.

B. Limitations

This study was constrained by the relatively small size of the development and evaluation datasets (60 recordings in total), and is intended as a proof-of-concept exploration of practical and methodological considerations for stationary human presence detection using radar. The dataset encompassed a broad range of conditions, including both indoor and outdoor environments, multiple target postures and distances, and the presence of both stationary and oscillating reflectors. While this diversity provides a measure of ecological validity, it also reduced statistical power, and consequently the reported classifier performance metrics should be interpreted as indicative only.

A more comprehensive data acquisition campaign would include a larger number of recordings collected across varied locations and under controlled repetitions, as well as distinct, previously unseen sites for evaluation to better emulate the deployment of a production-level radar system in unknown environments. Finally, this work employed an unsupervised machine-learning model specifically to contrast two conceptually distinct paradigms of detection: a conventional, hand-engineered threshold method based on physically interpretable features, and a purely data-driven approach that infers structure without labelled supervision. Supervised or semi-supervised models may have yielded better discrimination under these experimental conditions and may be more practically applicable.

C. Future Work

This exploratory study examined two distinct approaches to microwave-radar-based stationary human presence detection, but the potential directions for future development are numerous and depend on the intended application context. Regardless of the specific endpoint, future investigations would benefit from expanding the dataset size while maintaining, or further increasing, the environmental and target diversity achieved in this work. Evaluating multiple range gates, or extending the detection range window, would also enable closer emulation of real-world deployment scenarios.

For conventional threshold-based methods, future studies could focus on isolating the specific respiratory frequency peak within the radar phase signal and incorporating additional spectral descriptors into a multi-feature classification framework. Although a multi-feature threshold classifier was briefly explored here, it did not yield improved discrimination performance, as can be expected given the limited classification abilities of the individual features, and thus those results were not shown.

For machine-learning approaches, supervised and semi-supervised models are likely to provide more practical solutions than fully unsupervised methods, as previously mentioned, and are an obvious avenue for further exploration. Other directions could also investigate domain adaptation and transfer-learning strategies, in which a model trained under one set of environmental conditions can be algorithmically adapted to perform reliably in new or previously unseen settings, thereby enhancing robustness to environmental and operational variability [26].

V. Conclusion

In this study, an off-the-shelf 24 GHz frequency-modulated continuous-wave (FMCW) radar was configured for stationary human presence detection, and a custom software interface was developed to enable real-time visualisation of analog-to-digital converter (ADC) signals, fast Fourier transform (FFT) spectra, and phase tracking within a 1.3–1.7 m detection range, with on-demand data recording capability [18]. This work contributes to the growing body of research on microwave-band radar sensing by systematically evaluating the challenges posed by indoor and outdoor environments to both conventional threshold-based and machine-learning detection strategies.

The results presented here demonstrate that in dynamic outdoor environments, micro-Doppler signatures are not uniquely human-specific. However, temporal phase variation—when used as a feature within a conventional threshold-based classifier and iteratively optimised—can still provide meaningful discriminability, underscoring the continued relevance of classical signal-processing methods alongside modern machine-learning approaches.

Our custom software interface, along with all signal-processing and machine-learning pipelines developed in this work, are open-source and freely available for research use and further methodological development [18]. This study underscores the robustness of low-power microwave radar for stationary human presence detection. The breadth of classical and machine-learning signal-processing strategies now available will accelerate the translation of this modality into applications that range from healthcare monitoring, to search-and-rescue, and human-safety technologies.

Acknowledgment

I am deeply indebted to Dr. Graham Brooker of the Australian Centre for Robotics (University of Sydney) for his generous supervision and friendship during this project.

References

[1] M. T. Buyukakkaslar, M. A. Erturk, and M. A. Aydin, "A review on radar-based human detection techniques," *Sensors*, vol. 24, no. 17, 2024. [Online]. Available: https://www.mdpi.com/1424-8220/24/17/5709

[2] D. Shi, G. Gidion, L. M. Reindl, and S. J. Rupitsch, "Automatic life detection based on efficient features of ground-penetrating rescue radar signals," *Sensors*, vol. 23, no. 15, 2023. [Online]. Available: https://www.mdpi.com/1424-8220/23/15/6771

[3] G. Brooker, *Introduction to Sensors for Ranging and Imaging*. The Institution of Engineering and Technology, 2009. [Online]. Available: https://digital-library.theiet.org/doi/abs/10.1049/SBRA014E

[4] J. Cha, K. Yoo, D. Choi, and Y. Kim, "Human presence detection using ultrashort-range fmcw radar based on dcnn," *IEEE Sensors Journal*, vol. 24, no. 16, pp. 26 258–26 265, 2024.

[5] N. Kathuria and B.-C. Seet, "24 ghz flexible antenna for doppler radar-based human vital signs monitoring," *Sensors*, vol. 21, no. 11, 2021. [Online]. Available: https://www.mdpi.com/1424-8220/21/11/3737

[6] N. Regev and D. Wulich, "Radar-based, simultaneous human presence detection and breathing rate estimation," *Sensors*, vol. 21, no. 10, p. 3529, 2021.
[7] A. Whitworth, R. R. Bozorgzadeh, and J. A. Smith, "Characterization technique for a doppler radar occupancy sensor," *Electronics*, vol. 12, no. 24, p. 4888, 2023.
[8] D. Deiana, M. Gottardi, P. Ricci, P. Rocca, and R. Vescovo, "Real-time indoor presence detection with a novel radar-on-a-chip," in *2014 IEEE Radar Conference*, 2014, pp. 0304–0309.
[9] M. I. Skolnik, *Radar Handbook*, 3rd ed. New York: McGraw-Hill, 2008.
[10] P. Lang, X. Fu, M. Martorella, J. Dong, R. Qin, X. Meng, and M. Xie, "A comprehensive survey of machine learning applied to radar signal processing," 2020. [Online]. Available: https://arxiv.org/abs/2009.13702
[11] X. Li, Y. He, and X. Jing, "A survey of deep learning-based human activity recognition in radar," *Remote Sensing*, vol. 11, no. 9, 2019. [Online]. Available: https://www.mdpi.com/2072-4292/11/9/1068
[12] Google Cloud, "What is unsupervised learning?" 2024, accessed: 2025-11-05. [Online]. Available: https://cloud.google.com/discover/what-is-unsupervised-learning
[13] K. Papadopoulos and M. Jelali, "A comparative study on recent progress of machine learning-based human activity recognition with radar," *Applied Sciences*, vol. 13, no. 23, 2023. [Online]. Available: https://www.mdpi.com/2076-3417/13/23/12728
[14] Silicon Radar GmbH, *Evaluation Kit SiRad Easy® r4, SiRad Easy® & SiRad Simple® User Guide*, indie Semiconductor FFO GmbH, Im Technologiepark 1, 15236 Frankfurt (Oder), Germany, Nov. 2021, release 19-Nov-2021. Formerly Silicon Radar GmbH, now indie Semiconductor FFO GmbH. [Online]. Available: \url{https://www.siliconradar.com/datasheets/User_Guide_Easy_Simple_V2.5.pdf}
[15] Silicon Radar GmbH, *Product Sheet: SiRad Easy® r4 Radar Front End (RFE) Board TRX_024_046*, indie Semiconductor FFO GmbH, Im Technologiepark 1, 15236 Frankfurt (Oder), Germany, Mar. 2021, release 22-Mar-2021. Formerly Silicon Radar GmbH, now indie Semiconductor FFO GmbH. [Online]. Available: \url{https://www.siliconradar.com/datasheets/Product_Sheet_SiRad_Easy_r4_RFE_TRX_024_046_V1.0.pdf}
[16] Silicon Radar GmbH, *Evaluation Kit SiRad Easy® r4 System and Protocol Description*, indie Semiconductor FFO GmbH, Im Technologiepark 1, 15236 Frankfurt (Oder), Germany, Jan. 2023, release 23-Jan-2023. Formerly Silicon Radar GmbH, now indie Semiconductor FFO GmbH. [Online]. Available: https://www.siliconradar.com/datasheets/Protocol_Description_Easy_r4_V1.2.pdf
[17] Silicon Radar GmbH, *Evaluation Kit SiRad Easy® / SiRad Simple® WebGUI User Guide*, indie Semiconductor FFO GmbH, Im Technologiepark 1, 15236 Frankfurt (Oder), Germany, Apr. 2021, release 26-Apr-2021. Formerly Silicon Radar GmbH, now indie Semiconductor FFO GmbH. [Online]. Available: https://www.siliconradar.com/datasheets/User_Guide_WebGUI_Easy_Simple_V1.0.pdf
[18] Y. Yau, "Stationary human presence detection – python source code," https://github.com/yunkiyau/stationary-human-presence-detection, 2025, accessed: 10 Nov. 2025.
[19] A. Lerch, *An Introduction to Audio Content Analysis: Applications in Signal Processing and Music Informatics*. Hoboken, NJ: Wiley-IEEE Press, 2012.
[20] P. Stoica and R. L. Moses, *Spectral Analysis of Signals*. Upper Saddle River, NJ: Prentice Hall, 2005.
[21] W. J. Youden, "Index for rating diagnostic tests," *Cancer*, vol. 3, no. 1, pp. 32–35, 1950.
[22] scikit-learn developers, *Principal Component Analysis (PCA) — scikit-learn Documentation*, 2024, accessed: 10 Nov. 2025. [Online]. Available: https://scikit-learn.org/stable/modules/decomposition.html#pca
[23] scikit-learn developers, *sklearn.ensemble.IsolationForest — scikit-learn Documentation*, 2024, accessed: 10 Nov. 2025. [Online]. Available: https://scikit-learn.org/stable/modules/generated/sklearn.ensemble.IsolationForest.html#sklearn.ensemble.IsolationForest
[24] H. Research, "Diagnosing hong kong: The first smart hospital – cuhk mc," HKTDC Research Article, 18 August 2021, 2021, interview and description of the Chinese University of Hong Kong Medical Centre opening and its smart-hospital technologies. [Online]. Available: https://research.hktdc.com/en/article/ODE5NDEwNTAz
[25] GSMA, HKT, and CUHK Medical Centre, "5g: Enabling digital healthcare – cuhk mc smart hospital case study," GSMA 5G Case Studies, February 2022, 2022, case study on HK's first fully digitalised smart hospital, CUHK MC, including 5G/IoT/IoMT infrastructure. [Online]. Available: \url{https://www.gsma.com/solutions-and-impact/technologies/internet-of-things/wp-content/uploads/2022/02/2022-02-GSMA-APAC-5G-Case-Study-HKT-CUHKMC-5G-Smart-Hospital.pdf}
[26] S. J. Pan and Q. Yang, "A survey on transfer learning," *IEEE Transactions on Knowledge and Data Engineering*, vol. 22, no. 10, pp. 1345–1359, 2010.

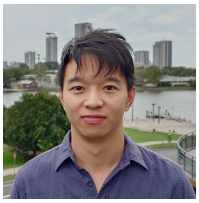

Yunki Yau is a BSc(Advanced) student at the University of Sydney. He has completed his Physics major and is in the first year of his Computer Science minor.